*Eastern Region Technical Attachment*
*No. 2008-03*
*April 2008*

# MULTI-YEAR EXAMINATION OF DENSE FOG AT BURLINGTON INTERNATIONAL AIRPORT

*John M. Goff*
*NOAA/National Weather Service*
*Burlington, VT*

## Abstract

An examination of the occurrence of dense fog at Burlington International Airport (KBTV) is performed in an effort to understand the synoptic signals that favor its formation, and to improve aviation forecasts of low instrument flight rule conditions at the site. Hourly weather data at KBTV from January 1979 through December 2003 (24 years) is used to identify all dense fog events (surface visibility less than ½ statute mile). Each event is then classified by type, reflecting the mechanism responsible for its formation. Six fog types are identified, with data indicating that 94% of all events may be categorized as radiation fog, precipitation induced fog, or fog resulting from lowering cloud bases. From this, frequency distribution and wind rose plots are constructed, showing distinct time periods within each year in which the three dominant fog types are favored. For precipitation induced fog and fog occurring from the lowering of cloud bases, clear directional wind trends from the northwest are observed. For radiation fog events directional wind trends are noted from the northeast. Further, analysis of mean sea level pressure (mslp) across the eastern United States is performed at the time of onset for each dominant fog event using National Weather Service, North American Regional Reanalysis (NARR) data. Several synoptic patterns are identified that favor each type, including 1) a mean anticyclone center to the north or west during radiation fog events, 2) the approach of a warm front, the passage of a cold or occluded front, and 3) the track of a surface cyclone south and east of KBTV. Finally, antecedent precipitation data for KBTV is analyzed before each radiation fog event to ascertain whether moist ground conditions played a supportive role in its formation. The results are encouraging, indicating 58% of events are preceded by precipitation within 24 hours. Using these results, it is argued that proper identification of the synoptic signals favorable to the formation of the three dominant fog types will aid the operational forecaster in identifying the potential for dense fog at Burlington International Airport, and thereby improve short term aviation forecasts at this site.

## 1. Introduction

Among the most challenging weather phenomena to predict for the short-term forecaster on an annual basis is that of dense fog. Despite improvements in forecasting techniques during recent years, the ability to predict the time of onset, degree of coverage, and time of dissipation of fog remains difficult at best for many locales. This is especially true at sites where it does not occur on a regular basis. The importance of improving short-term forecasts of dense fog is paramount when one considers the safety hazard posed to the transportation community and the overall economic loss for the aviation and shipping industries annually due to delays caused by its occurrence. Widespread investigative research into the causes and mechanisms responsible for the formation of dense fog has only begun within the past 20 years. Many of these studies focused on local climatologies or discrete events (Slemmer 2004; Tardif et al. 2004), while others addressed fog climatology on a more regional scale (Westcott 2004; Tardif 2004). In another study, Croft et al. (1997) developed a conceptual model approach to dense fog forecasting across the southern portions of the U.S., using both climatology and model diagnostic software.

It is argued that proper identification of the synoptic signals favorable to the formation of dense fog is critical in day-to-day short-term weather forecasts within the National Weather Service (NWS). It is the objective of this study to aid the forecaster in identifying the signals unique to KBTV. This will foster better recognition of the potential for dense fog more readily, thereby improving short term aviation forecasts at the site.

To this end, a comprehensive 24-year analysis of all dense fog (surface visibility < ½ statute mile) events is performed at Burlington International Airport (KBTV) using hourly weather data (January 1979 through December 2003) in an effort to understand the climatology of the phenomenon, to explore the possible synoptic signals that favor its formation, and ultimately to improve aviation forecasts of low instrument flight rules (LIFR, defined as ceilings less than 500 feet and/or surface visibility less than 1 mile) at the site. After identifying all dense fog occurrences, discrete events are then classified into six types, similar to those noted in Tardif (2004), in order to identify the mechanism responsible for formation. Of these six, it was noted that 94% of all fog cases fell into three distinct types, specifically, radiation fog (RF), fog induced by falling precipitation (PF), and fog formed from the lowering of cloud base (LCB). Thus, remaining focus will be drawn from this smaller subset. Using climatological frequency distribution analysis, wind rose plots, and mean sea level pressure charts from the North American Regional Reanalysis (NARR) dataset (Mesinger et al. 2006), distinct characteristics are outlined for each of the aforementioned three fog types. Finally, antecedent precipitation within 24 hours of each type RF event is examined to determine whether residual moist ground conditions (i.e. saturation of the nocturnal boundary layer) play a critical role in dense fog formation.

The remainder of the paper will address the specific details described above. Section 2 contains a description of the data sources and software used to examine each event, while Section 3 highlights specific findings and forecasting suggestions resulting from their use. Finally, Section 4 draws on these

earlier results to highlight conclusions that can be drawn from the data.

## 2. Data and methodology

Hourly weather data for a 24-year period, spanning January 1979 through December 2003, was used to identify all observed cases of dense fog at KBTV. This time period was chosen as it correlated well with available NARR data for the site. An event was determined to occur at the airport if surface visibility was less than ½ statute mile for at least one hour. Examination of the data indicated 344 total events during the period, or an average of approximately 14 events per year. A classification scheme similar to that used by Tardif (2004) was then performed on each event in order to determine the fog's character, and the processes by which it formed. Six discernable fog types were identified (Fig. 1), including those induced by the following processes: radiation (RF), advection (AF), falling precipitation (PF), lowering of cloud base (LCB), evaporation of surface moisture at sunrise (EF), and indeterminate factors (IF). It was noted that 94% of all cases fell under the classifications of RF, PF, and LCB, and as such the focus of this study is centered on these three dominant fog type classifications.

To ascertain the annual monthly distribution of the three dominant fog types at KBTV, all categorized events were summed and tallied by month over the 24-year period. Frequency distribution plots were then constructed accordingly. Additionally, to determine the frequency distribution of wind direction and speed for each of the three primary fog types, comprehensive wind rose plots were constructed using *WRPLOT View* software (Version 5.0, Lakes Environmental Software 2005:, accessible from: http://www.lakesenvironmental.com/lakewrpl.html). In order to evaluate possible synoptic scale signals inherent during a dominant type of fog event at KBTV, mean sea level pressure plots were constructed for each event type (RF, PF, and LCB) using online data obtained from NCEP's North American Regional Reanalysis (NARR) dataset. Data are available in three hour time increments, with plot times corresponding to the three hour time step which most closely matched the time of fog onset in each event. Composite analysis of the plots was then generated to ascertain whether any signals were inherent in the data. Frequency distribution plots were then constructed accordingly.

In accordance with similar studies (Shaffer 2007), it was queried as to whether antecedent precipitation played a supportive role in the formation of dense radiation fog (RF) at KBTV. Antecedent 12-, 24-, and greater than 24-hour precipitation was recorded for all RF events observed, and frequency distribution data then plotted for each case. Measurable precipitation was regarded as a liquid measurement of 0.01 inches or greater, in accordance with National Weather Service Instruction 10-1302, 2005: (accessible from: http://www.weather.gov/directives/sym/pd01013002curr.pdf).

## 3. Results

*a. Frequency distribution and wind rose plots*

Analyses of frequency distribution plots for the three dominate fog types described in the previous section show distinct climatological periods within each year that favor their formation. For RF events, a clear maximum is evident during the late summer

and early fall (August through October), while a lesser secondary maximum is noted during June (Fig. 2). A broad minimum in RF occurrence was noted during the cool season (November through March). As a whole, RF events comprise approximately 34% of all events, or around 5 events per year. For types PF and LCB, a broad maximum was noted throughout the cool season (November through April), while a minimum in occurrence was noted during the warm season months (May through October). The data indicate that PF events comprise 52% of all cases identified, whereas LCB events comprise 8%. Due to the similarity in the monthly frequency distributions of type PF and LCB events, and that approximately 60% of all dense fog events at KBTV fall under these two types, the two groups were paired together in the plots for clarity.

Frequency distribution analysis of the mean wind fields associated with each of the three dominant fog types noted at KBTV was then performed using wind rose plots. Clear and distinct directional trends were evident with each type. For RF events, a strong directional signal was observed from the northeast to east, with approximately 65% of all observed events falling within the 045 to 135 degree sector (Fig. 3). About 25% of observed RF events were associated with calm winds, with the remaining events (about 10%) associated with wind directions outside of the 045 to 135 degree sector, mainly from the north. Examination of the wind class frequency distributions of RF events shows that 97.5% of all observations occur with wind speeds less than or equal to 4 knots, with only 2.5% occurring with wind speeds of 5 knots (Fig. 4).

For combined type PF and LCB events, the wind rose analysis again exhibited clear directional signals, with approximately 65% of observed events in the 24-year period falling within the 290 to 360 degree sector, or having a direction primarily from the northwest to north (Fig. 5). Approximately 9% of observed events were noted as having calm winds, while the remaining 26% fell outside the aforementioned 290 to 360 degree sector, generally from a southerly direction. Investigation of the wind class frequency distribution plots of combined type PF and LCB events yielded a varying assortment of wind speeds, with a distribution centered about the 5 to 10 knot wind class (Fig. 6).

*b. NARR analysis*

Composite analysis of mean sea level pressure (mslp) plots of each RF, PF, and LCB event were performed nearest to the time of fog onset. For RF events, 92% of all observances were coincident with a surface anticyclonic ridge axis across northern Vermont (Fig. 7). These cases were then determined to fall into two sub-groups, with one cluster showing a mean anticyclonic center north to northwest of KBTV, and the other showing a mean anticyclonic center to the west or southwest of KBTV (Figs. 8-10). The remaining 8% of RF events were categorized as indeterminate (Figs. 7 and 10).

For the combined group of types PF and LCB, three synoptic surface patterns were identified and associated with fog development (Fig. 11). These were: (1) the passage of an occluded or cold front, (2) the approach of a warm front, and (3) the positioning of KBTV within the northwestern quadrant of a surface cyclone (Figs. 12-14). Of these patterns, the positioning of KBTV deep on the northwest flank of a surface cyclone appeared most

favorable, with this setup occurring in 47% of all observed cases (Fig. 11). The remaining 53% were divided nearly equally between occluded/cold frontal passages, and the approach of a warm frontal boundary.

*c. Antecedent precipitation data*

Similar to Shaffer (2007), 12- and 24-hour antecedent precipitation data were analyzed for each RF event identified. The data indicated that over half (58%) of all RF events were preceded by measurable precipitation within 24 hours of fog onset, and nearly one third (31%) were preceded by measurable precipitation within 12 hours (Fig. 15).

## 4. Discussion

*a. Forecasting RF events*

Of all signals associated with radiation fog at KBTV, the light east to northeasterly drainage wind identified in the wind rose plots appears to be most significant, as only 10% of all events occur with wind directions outside of the 045 to 135 degree sector (Fig. 3). A brief examination of the local topography at KBTV provides substantial insight into the most likely cause of RF events at KBTV under these wind conditions. KBTV is situated on a flat hilltop at approximately 340 feet above mean sea level. The Winooski River valley lies to the immediate east and northeast of the site, and is some 200 feet lower than the airport (Fig. 16). The valley experiences dense radiation fog on numerous nights from late summer through early autumn as cold air drainage from the land surface occurs over the relatively warm river water. Thus a light northeasterly wind direction would certainly favor transport of the fog south and west across KBTV should it form in the valley. It has been noted that large differences between ambient air and river water temperatures may lead to saturation of the boundary layer and subsequent fog formation in vicinity of the river (Croft et al. 1997). Croft et al. (1997) identified one such case. However, applying this hypothesis locally is limited due to the lack of recorded surface water temperature data in the Winooski River near KBTV and the extent to which air-water temperature differences drive local fog formation. Additional support is provided in the NARR mean sea level pressure analysis of each RF event. As noted earlier, composite plots indicated that surface anticyclonic ridging was oriented across northern Vermont during 92% of all observed RF events (Fig. 7). Individual cases showing typical mean sea level pressure patterns associated with RF events at KBTV are shown in figures 8-10. This synoptic pattern supports a light drainage wind regime, with broad subsidence atop a shallow and potentially moist nocturnal boundary layer. The topographical orientation of the Winooski River valley ensures that the favored drainage wind direction at KBTV is from the northeast during these synoptic regimes.

Despite favorable synoptic signals, dense radiation fog is not a common occurrence at KBTV given its prevalence in the river valley to the immediate east and northeast. It was hypothesized that perhaps the depth and relative saturation of the nocturnal boundary layer could potentially play a significant role, provided the other dominant signals were present. Accordingly, antecedent precipitation data was examined at KBTV within 12, 24, and more than 24 hours before each RF event. Though not conclusive, the data showed that approximately 58% of all events were preceded by measurable precipitation within

24 hours, and 31% within 12 hours (Fig. 15). This appears to support the hypothesis that residual surface moisture contributes to a more thorough saturation of the nocturnal boundary layer under light drainage wind regimes. Provided the depth of the layer is greater than 200 feet, a favorable setup for an RF event occurrence at KBTV is more likely given the presence of clear skies and a light northeast drainage wind.

Analysis of the annual frequency distribution plot of RF events was also quite conclusive, with a majority of events occurring during the three month period of August through October (Fig. 2). This is to be expected, when optimal conditions of a longer nocturnal period, radiational cooling and ample surface moisture occur more often. Therefore, consideration should be given to the time of year when forecasting an RF event at KBTV. Finally, the forecaster should consider the fact that RF events comprised approximately 34% of all dense fog events noted at KBTV during the 24 years of this study (Fig. 1). With 14 dense fog events per year on average, this corresponds to only five (5) RF events per year at the airport. With RF events occurring so infrequently at KBTV, conditional climatology-based tools and Model Output Statistical (MOS) guidance are often of little help, and discretion is advised when attempting to forecast dense RF events at KBTV beyond 12 hours, even if the aforementioned synoptic and mesoscale signals are present.

*b. Forecasting PF/LCB events*

In similar fashion to RF events, the wind rose analysis of combined PF and LCB events appeared to be the most significant. Though the plots exhibited a distribution in wind speeds centered around the 5 to 10 knot wind class (Fig. 6), a clear directional signal from the northwest to north was evident in the dataset, with approximately 65% of all events falling within the 290 to 360 degree sector (Fig. 5). To better understand why dense fog is more prevalent at KBTV under north to northwest flow regimes, one must consider the topographical orientation of the northern Champlain Valley. Figure 17 shows that the Green and Adirondack mountains that encompass the valley to the east and west, respectively, converge slightly from the Canadian border southward. Forced slightly inward by topography, northerly flow in the northern portions of the valley is subsequently confluent and is often associated with low cloud cover and precipitation, especially during the fall and winter months under moist boundary layer conditions. It is proposed that this topographically influenced confluent northerly flow is a primary factor when considering a forecast of dense PF or LCB fog. This is especially true when frozen precipitation such as snow is expected, which may significantly reduce visibility.

Analysis of the NARR mean sea level pressure data for each PF and LCB event yielded key signals as well. As discussed above, three primary synoptic conditions were identified under which predominant north or northwesterly flow occurred. These were: (1) the passage of an occluded or cold front, (2) the approach of a warm front, and (3) the positioning of KBTV within the northwest quadrant of a surface cyclone. Individual cases illustrating these typical patterns are shown in figures 12-14. Of these, nearly half (47%) occurred on the northwestern flank of a surface cyclone, with the remaining 53% satisfying the other two conditions (Fig. 11). The higher percentages identified in the surface cyclone

cases appears reasonable, as mean boundary layer flow is more typically cyclonic under such regimes, and columnar moisture profiles are often deeper, leading to more efficient hydrometeor generation.

Finally, analysis of annual frequency distribution plots of combined PF and LCB events showed that this group exhibited a broad maximum throughout the cold season (November through April), and a distinct minimum during the warm season months (May through October). Though of lesser importance, the data indicate that time of year certainly plays a role in the development and evolution of PF and LCB events at KBTV when cyclonic, convergent, cold advection processes occur more frequently. Using this information, it is evident that when considering PF or LCB conditions at KBTV, the forecaster must assess several factors in order to gain a better grasp of the overall synoptic setup. It is also worthy to note that despite comprising 60% of all dense fog events, PF and/or LCB events occur on average only nine (9) times annually at KBTV. Therefore, discretion is again advised in attempting to forecast these events at KBTV beyond 12 hours.

## 5. Conclusion

It has been shown that despite its relatively infrequent occurrence at Burlington International Airport, dense fog can be linked to several key synoptic patterns. For radiation fog, this would include: (1) mean surface high pressure atop the region, centered generally to the north or northwest, (2) light northeasterly surface drainage flow, (3) a favored time period during the warm season months (August through October), and (4) possibly antecedent precipitation at the site. For fog induced by falling precipitation, or that occurring from lowering ceiling heights, signals include: (1) mean north to northwest boundary layer flow, (2) a synoptic position associated with the approach or passage of a warm front, cold or occluded front, or a surface cyclone, and (3) a favored time period during the cold season months (November through April). By identifying these signals during the appropriate time of year, the operational forecaster may gain insight into the potential for dense fog formation at the site. To this end, a decision tree or similar tool on fog formation may be useful. This will hopefully lead to improved short term (within 12 hours) aviation forecasts of LIFR conditions.

## Acknowledgements

The author would like to thank Paul Sisson, Science and Operations Officer at the NWS in Burlington, VT, and John DiStefano, Science and Operations Office at the NWS in Wilmington, OH for their overall guidance and oversight during this process. Thanks are also given to Conor Lahiff, meteorologist at the NWS in Burlington, VT for his help with plotting techniques using the wind rose software.

## Disclaimer

Mention of a commercial company or product does not constitute an endorsement by the National Weather Service. Use of information from this publication concerning proprietary products or tests of such products for publicity or advertising purposes is not authorized.

## References


Croft, P.J., R.L. Pfost, J.M. Medlin, and G.A. Johnson, 1997: Fog forecasting for the Southern Region: A conceptual model approach. *Wea. Forecasting*, **12**, 545-556.

Mesinger, F., and Co-authors, 2006: North American regional reanalysis. *Bull. Amer. Meteor. Soc.*, **87,** 343-360.

Shaffer, W., 2007: Dense fog study for Knoxville, Tennessee. National Weather Service, Morristown, TN. [Unpublished manuscript available on-line from http://www.srh.noaa.gov/mrx/research/Fog/fogtys.php]

Slemmer, J., 2004: Study of dense fog at the Salt Lake City International Airport and its impacts to aviation. *National Weather Service Technical Attachment*, 2004-01.

Tardif, R., 2004: Characterizing fog occurrences in the Northeastern United States using historical data. Preprints, *11th Conf. on Aviation, Range and Aerospace Meteorology*, Hyannis, MA. Amer. Meteor. Soc., Paper 10.6.

----------, J.A. Cole, P.H. Herzegh, S.D. Landolt, R.M. Rasmussen, M.L. Tryhane, 2004: First observations of fog and low ceiling environments at the FAA Northeast ceiling and visibility field site. Preprints, *11th Conf. on Aviation, Range and Aerospace Meteorology*, Hyannis, MA, Amer. Meteor. Soc., Paper 10.5.

Westcott, N., 2004: Synoptic conditions associated with dense fog in the Midwest. Preprints, *14th Conf. on Applied Climatology*, Seattle, WA, Amer. Meteor. Soc., Paper 2.4.

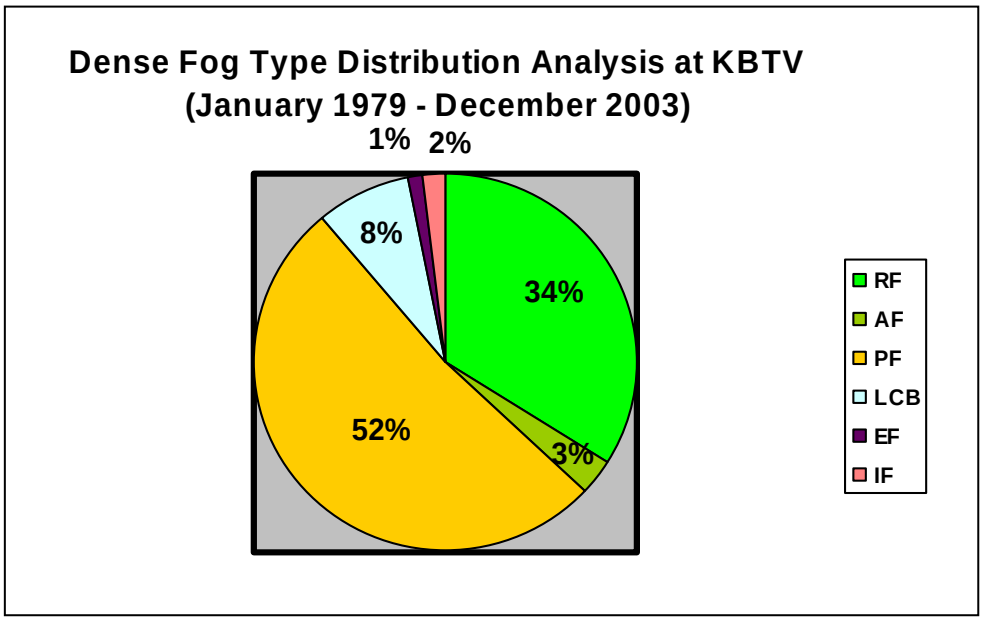


**Figure 1.** Annual distribution of dense fog type at KBTV during the 24-year period of the study. RF = radiation fog; AF = advection fog; PF = fog induced by falling precipitation; LCB = fog resulting from the lowering of cloud ceiling base; EF = fog caused by the evaporation of surface moisture at sunrise; IF = fog caused by indeterminate factors.

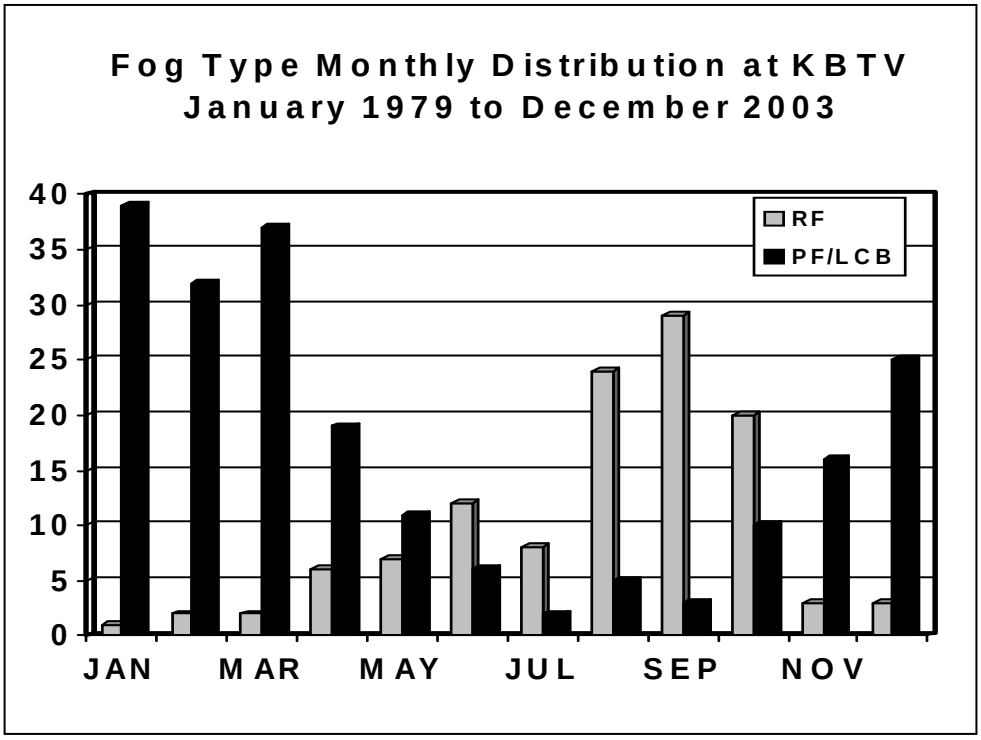


**Figure 2.** Monthly distribution of RF and the combined fog types of PF and LCB.

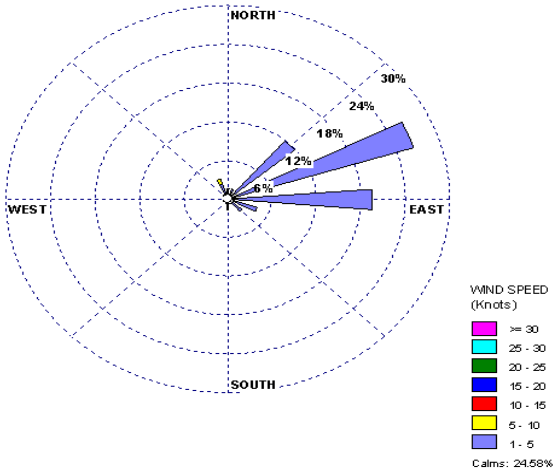


**Figure 3.** Directional wind rose plot of RF events at KBTV from Jan. 1979 to Dec. 2003.

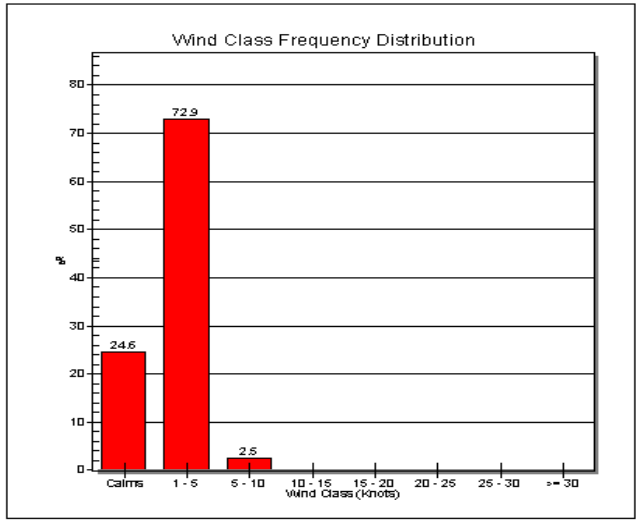


**Figure 4.** Wind speed frequency distribution of RF events at KBTV from Jan. 1979 to Dec. 2003.

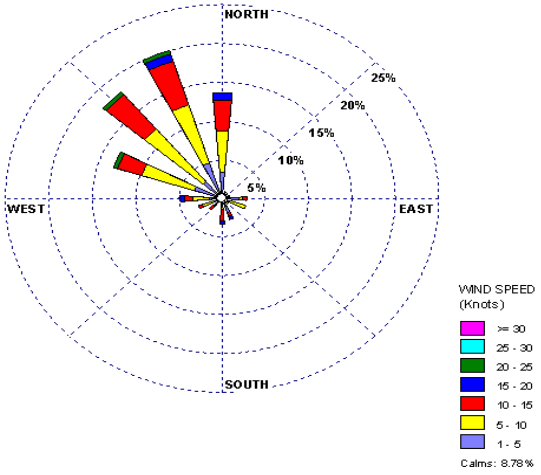


**Figure 5.** Directional wind rose plot of combined PF/LCB events at KBTV from Jan. 1979 to Dec. 2003**.**

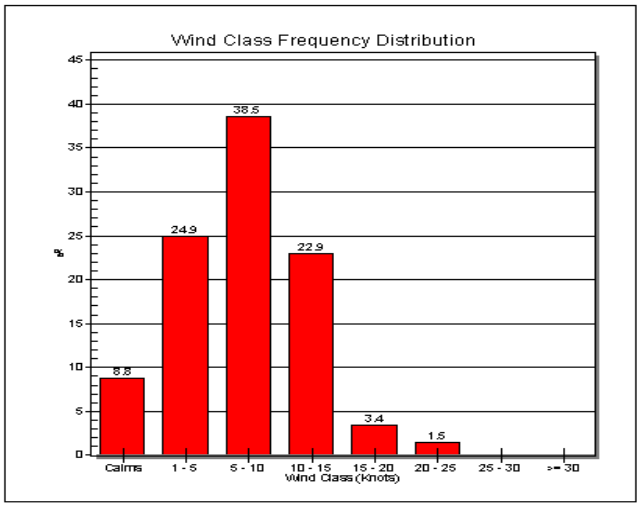


**Figure 6.** Wind speed frequency distribution of combined PF/LCB events from Jan. 1979 to Dec. 2003

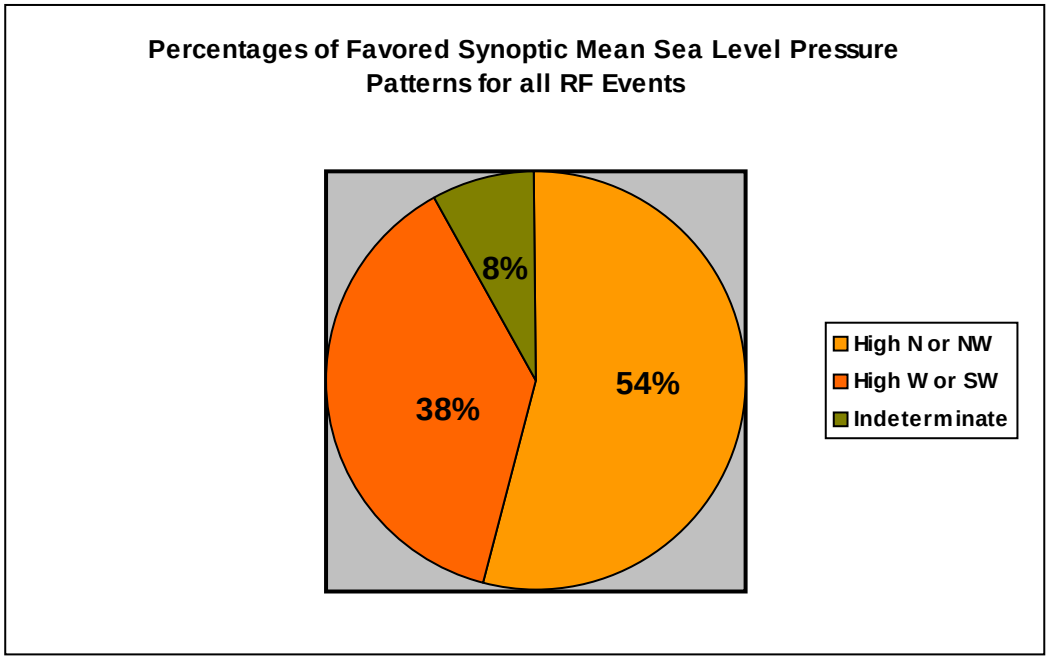


**Figure 7.** Distribution analysis of favored synoptic mean sea level pressure patterns associated with RF events at KBTV from Jan. 1979 to Dec. 2003.

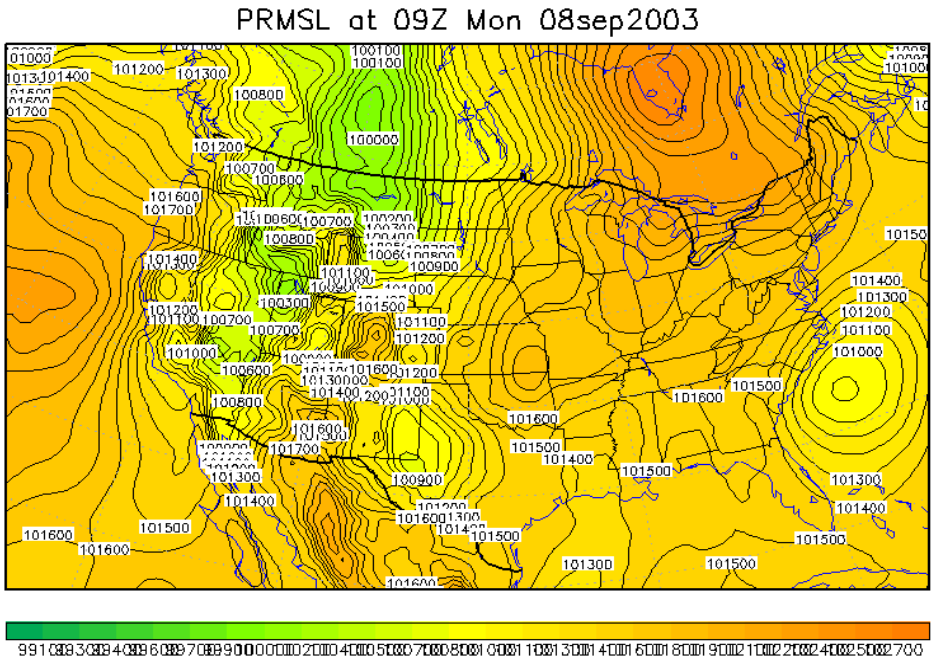


**Figure 8.** NARR mean sea level pressure analysis during an occurrence of an RF event at 0900 UTC 8 September 2003, showing surface anticyclone position to the north/northwest of KBTV (isobar units in hPa x $10^2$).

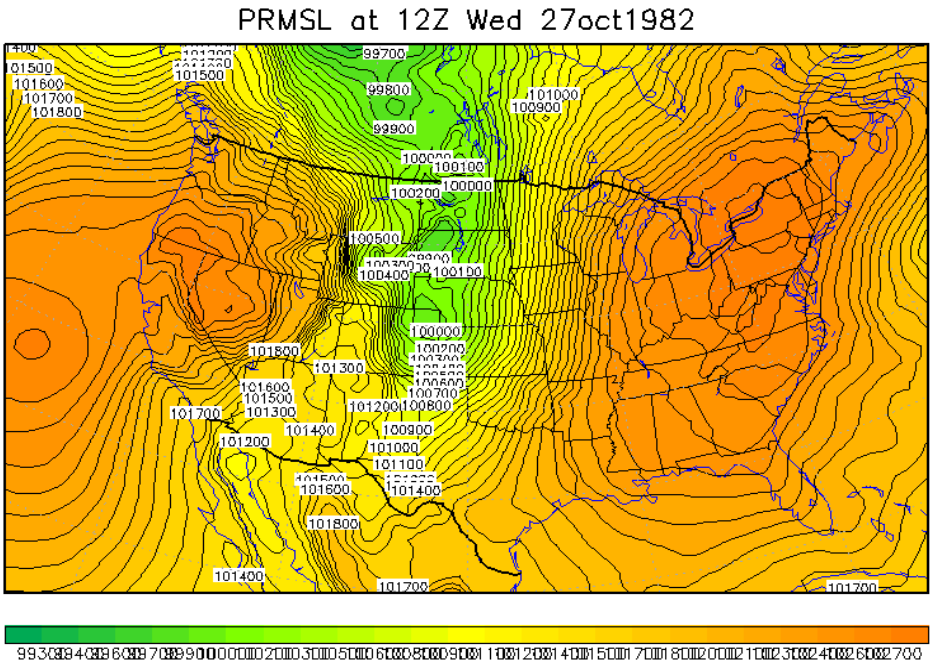


**Figure 9.** NARR mean sea level pressure analysis during an occurrence of an RF event at 1200 UTC on 27 October 1982 showing surface anticyclone position to the west/southwest of KBTV (isobar units in hPa x $10^2$).

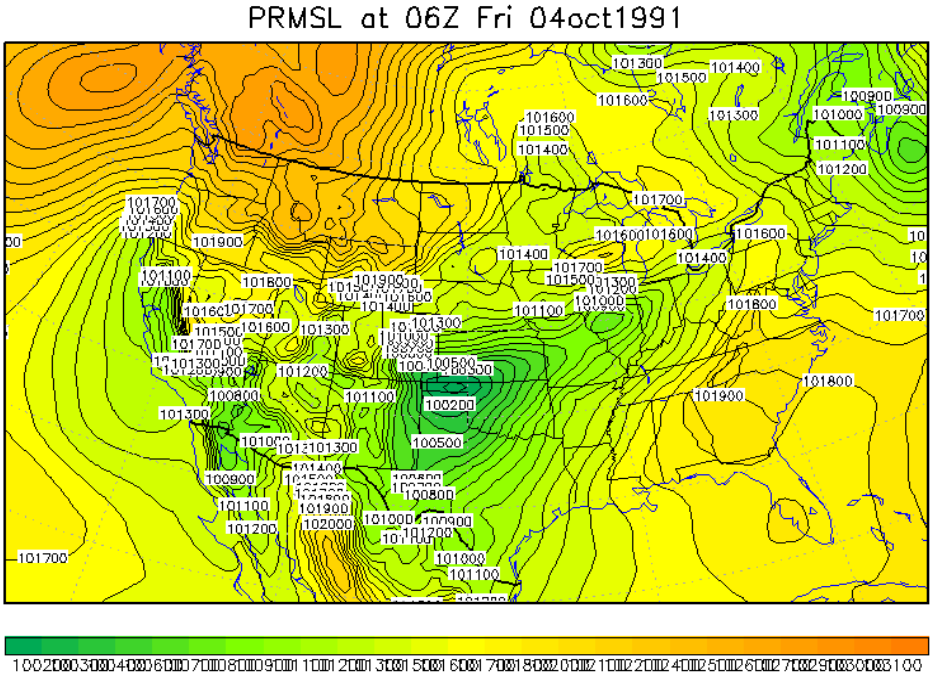


**Figure 10.** NARR mean sea level pressure analysis during an occurrence of an RF event at 0600 UTC 4 October 1991, showing an indeterminate cause and/or general lack of a mean surface anticyclone in the vicinity of KBTV (isobar units in hPa x $10^2$).

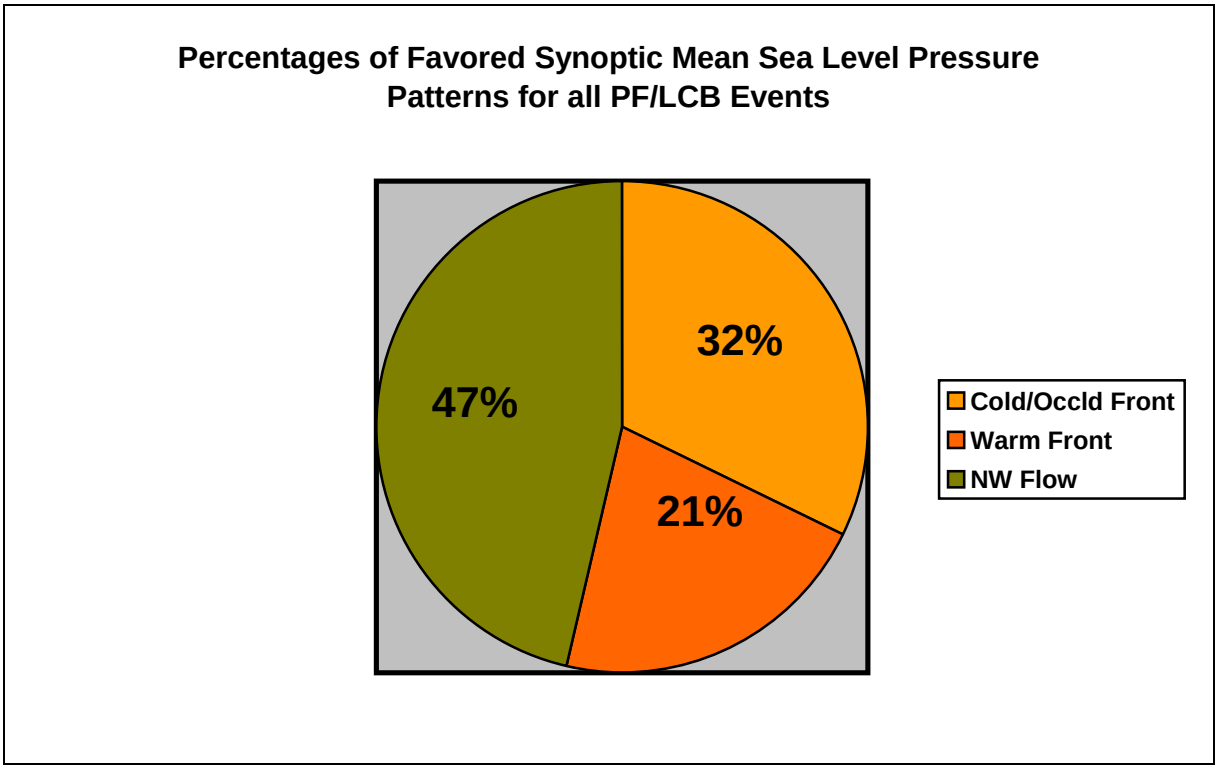


**Figure 11.** Distribution analysis of favored synoptic mean sea level pressure patterns associated with combined PF/LCB events at KBTV from Jan. 1979 to Dec. 2003.

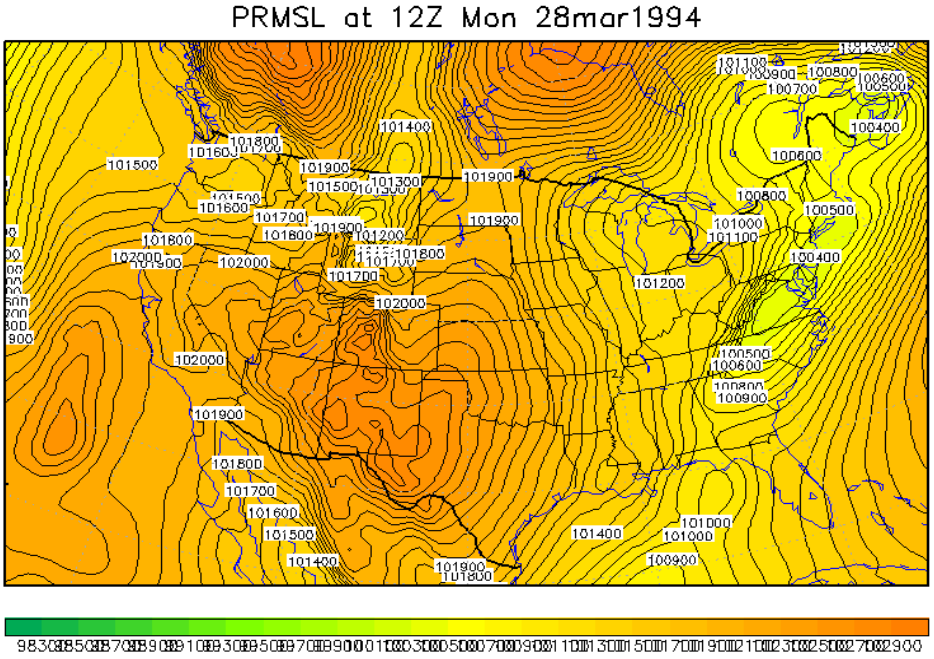


**Figure 12.** NARR mean sea level pressure analysis during an occurrence of a PF event at 1200 UTC 28 March 1994, showing a cold or occluded frontal passage at KBTV (isobar units in hPa x $10^2$).

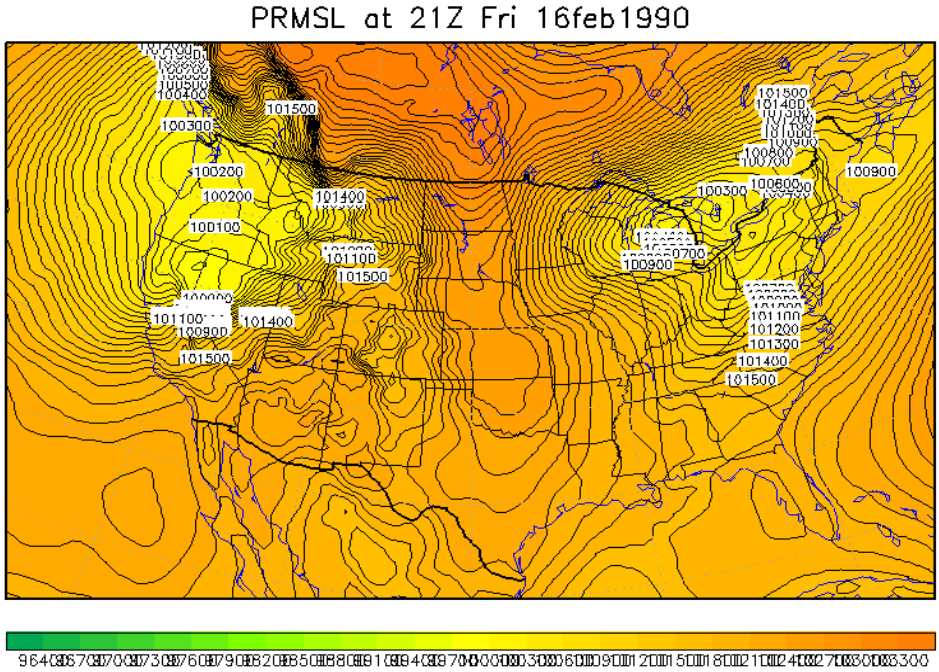


**Figure 13.** NARR mean sea level pressure analysis during an occurrence of an LCB event at 2100 UTC 16 February 1990, showing the approach or passage of a warm frontal boundary at KBTV (isobar units in hPa x $10^2$).

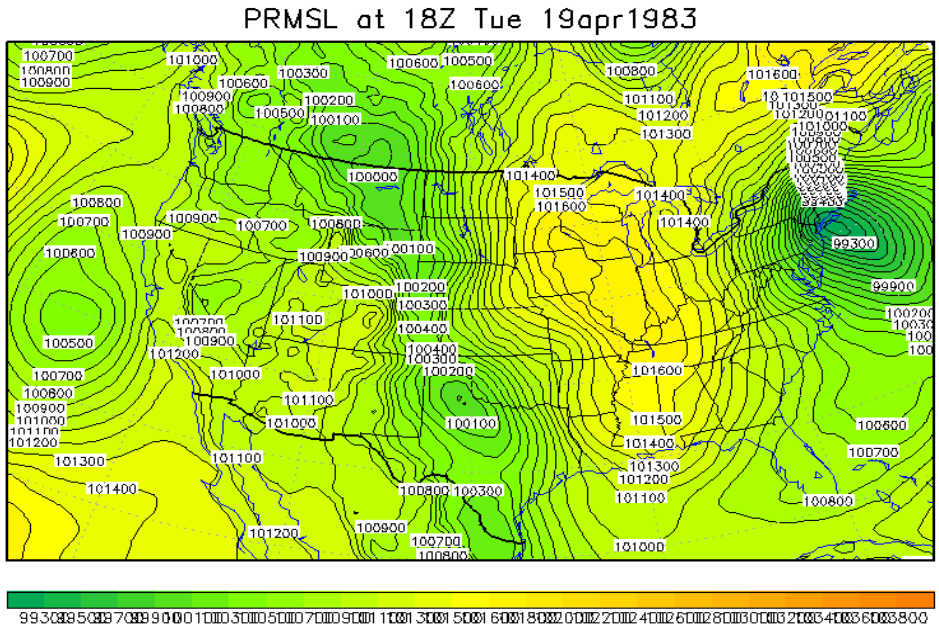


**Figure 14.** NARR mean sea level pressure analysis during an occurrence of a PF event at 1800 UTC 19 April 1983, showing north to northwest surface flow at KBTV on the northwest side of a surface cyclone (isobar units in hPa x $10^2$).

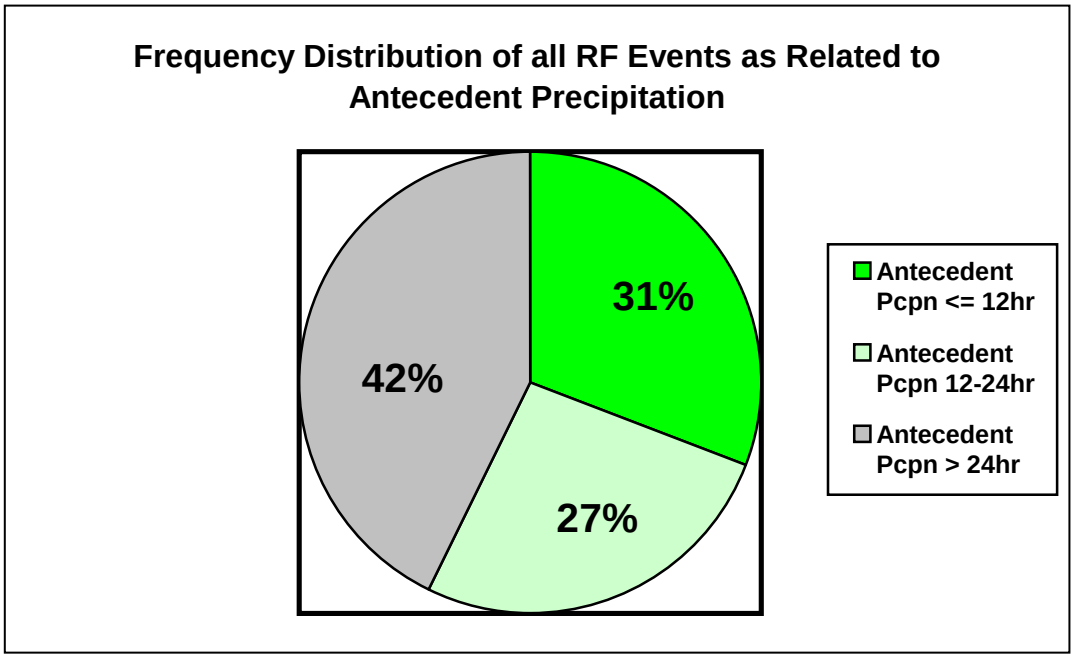


**Figure 15.** Frequency distribution of all RF occurrences at KBTV from Jan. 1979 to Dec. 2003 as related to antecedent precipitation.


**Figure 16.** Topographical map in vicinity of KBTV showing airport runway orientations (purple lines), ASOS location (red dot), and location of Winooski River (thick blue line).

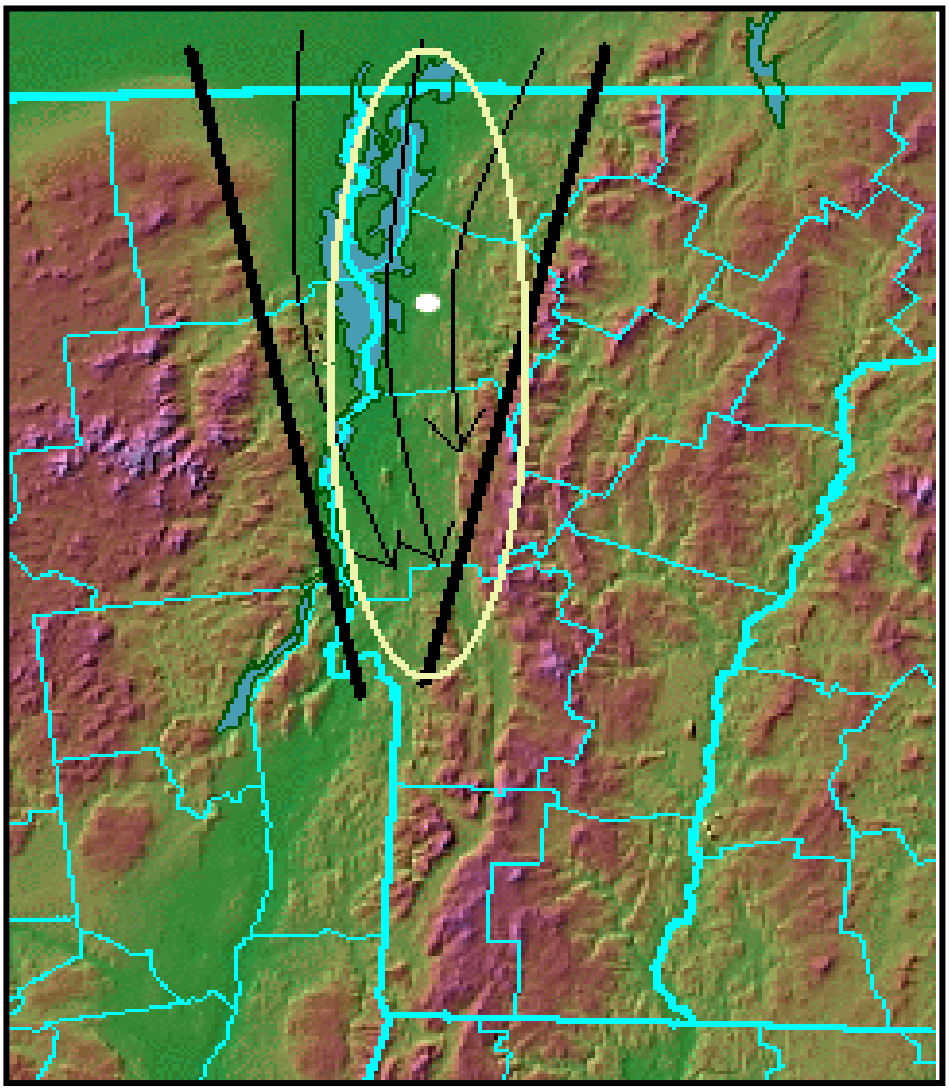

**Figure 17.** Topographical map of Champlain Valley (yellow ellipse) showing confluent mesoscale surface flow (arrows) produced under mean north to northwest wind regimes. Solid black lines indicate approximate eastern (western) extent of the Adirondack and Green mountains respectively, while KBTV is indicated by white dot.